Comparative Evaluation of the Translocator Protein Radioligands ^{11}C-DPA-713, ^{18}F-DPA-714, and ^{11}C-PK11195 in a Rat Model of Acute Neuroinflammation

Fabien Chauveau[1–3], Nadja Van Camp[1,2], Frédéric Dollé[1], Bertrand Kuhnast[1], Françoise Hinnen[1], Annelaure Damont[1], Hervé Boutin[1,2,4], Michelle James[5], Michael Kassiou[5–7], and Bertrand Tavitian[1,2]

[1]CEA, DSV, I2BM, LIME, Orsay, France; [2]INSERM, U803, Orsay, France; [3]CREATIS-LRMN, CNRS, UMR 5220, and INSERM, U630, Bron, France; [4]Faculty of Life Sciences, AV Hill Building, University of Manchester, Manchester, United Kingdom; [5]Brain and Mind Research Institute, University of Sydney, Sydney, New South Wales, Australia; [6]Discipline of Medical Radiation Sciences, University of Sydney, Sydney, New South Wales, Australia; and [7]School of Chemistry, University of Sydney, Sydney, New South Wales, Australia

Overexpression of the translocator protein, TSPO (18 kDa), formerly known as the peripheral benzodiazepine receptor, is a hallmark of activation of cells of monocytic lineage (microglia and macrophages) during neuroinflammation. Radiolabeling of TSPO ligands enables the detection of neuroinflammatory lesions by PET. Two new radioligands, ^{11}C-labeled N,N-diethyl-2-[2-(4-methoxyphenyl)-5,7-dimethylpyrazolo[1,5-α]pyrimidin-3-yl] acetamide (DPA-713) and ^{18}F-labeled N,N-diethyl-2-(2-(4-(2-fluoroethoxy)phenyl)-5,7-dimethylpyrazolo[1,5-α]pyrimidin-3-yl) acetamide (DPA-714), both belonging to the pyrazolopyrimidine class, were compared in vivo and in vitro using a rodent model of neuroinflammation. **Methods:** ^{11}C-DPA-713 and ^{18}F-DPA-714, as well as the classic radioligand ^{11}C-labeled (R)-N-methyl-N-(1-methylpropyl)-1-(2-chlorophenyl)isoquinoline-3-carboxamide (PK11195), were used in the same rat model, in which intrastriatal injection of (R,S)-α-amino-3-hydroxy-5-methyl-4-isoxazolopropionique gave rise to a strong neuroinflammatory response. Comparative endpoints included in vitro autoradiography and in vivo imaging on a dedicated small-animal PET scanner under identical conditions. **Results:** ^{11}C-DPA-713 and ^{18}F-DPA-714 could specifically localize the neuroinflammatory site with a similar signal-to-noise ratio in vitro. In vivo, ^{18}F-DPA-714 performed better than ^{11}C-DPA-713 and ^{11}C-PK11195, with the highest ratio of ipsilateral to contralateral uptake and the highest binding potential. **Conclusion:** ^{18}F-DPA-714 appears to be an attractive alternative to ^{11}C-PK11195 because of its increased bioavailability in brain tissue and its reduced nonspecific binding. Moreover, its labeling with ^{18}F, the preferred PET isotope for radiopharmaceutical chemistry, favors its dissemination and wide clinical use. ^{18}F-DPA-714 will be further evaluated in longitudinal studies of neuroinflammatory conditions such as are encountered in stroke or neurodegenerative diseases.

Because neuroinflammation plays a key role in various acute and chronic neuropathologic conditions, including stroke, brain trauma, Alzheimer disease, and Parkinson disease (1), a noninvasive imaging biomarker would greatly benefit the monitoring of these neurologic disorders and the development of therapies for them. The translocator protein (TSPO) (18 kDa), formerly known as the peripheral benzodiazepine receptor, is only modestly expressed in normal brain parenchyma but is dramatically upregulated during neuroinflammation, and this upregulation has been shown to correlate with the activation of microglial cells, or the infiltration of blood-borne macrophages (2). Targeting TSPO with radiolabeled ligands for PET or SPECT is a logical objective for the in vivo detection of the activation and migration of cells of monocytic lineage in the brain and is generally considered an attractive biomarker for neuroinflammation (3–5).

(R,S)-N-methyl-N-(1-methylpropyl)-1-(2-chlorophenyl)-isoquinoline-3-carboxamide (PK11195) was the first nonbenzodiazepine ligand for TSPO, and radiolabeled ^{11}C-PK11195 (6) has been extensively used for PET of neuroinflammation. However, human PET studies have repeatedly demonstrated difficulties in quantifying the binding potential (BP) of ^{11}C-PK11195 because of inadequate pharmacokinetic properties, poor bioavailability toward brain tissue, and a high level of nonspecific binding (7). In addition to these drawbacks, the short half-life of ^{11}C (20.4 min) is a

major limitation to the clinical dissemination of ^{11}C-PK11195, the longer half-life of [18]F (109.8 min) being preferred in order to facilitate both distribution and multiple use of the radiotracer production batches. The search for alternative ligands of TSPO has rapidly expanded (8), and more than 40 new compounds have been investigated at various levels of detail in experimental imaging studies (9). However, the large variability in experimental protocols and in animal models of neuroinflammation has prevented an objective comparison of these alternative radioligands. In addition, with regard to obtaining a better TSPO radiotracer than ^{11}C-PK11195, it appears reasonable to consistently compare the candidate TSPO radioligand with ^{11}C-PK11195 in similar animal models. Rat models are attractive in that they have a low cost, identical genetic backgrounds, and a sufficiently large brain for PET studies. However, the basal expression of TSPO in the rodent brain is low (10) and thus a robust model of neuroinflammation with a high target-to-background ratio is required for valuable screening of candidate radiotracers targeting TSPO.

We previously reported in vivo imaging of neuroinflammation of the pyrazolopyrimidine radioligand ^{11}C-labeled N,N-diethyl-2-[2-(4-methoxyphenyl)-5,7-dimethylpyrazolo[1,5-α]pyrimidin-3-yl]acetamide (DPA-713) in rats bearing an excitotoxic striatal lesion (11). Recently, ^{18}F-labeled N,N-diethyl-2-(2-(4-(2-fluoroethoxy)phenyl)-5,7-dimethylpyrazolo[1,5-α]pyrimidin-3-yl)acetamide (DPA-714), an ^{18}F-labeled derivative, demonstrated TSPO specificity and interesting biodistribution properties in primates (12). In the present paper, we report in vitro autoradiography and in vivo PET of ^{18}F-DPA-714 in comparison to ^{11}C-PK11195 and ^{11}C-DPA-713 (Fig. 1) in the same excitotoxic model of neuroinflammation. This direct comparison of ^{18}F-labeled DPA-714 with its ^{11}C analog DPA-713 and with ^{11}C-PK11195 supports the view that ^{18}F-DPA-714 is a most promising PET radiotracer for TSPO imaging.

MATERIALS AND METHODS

Animal Model

Forty-three Wistar rats (250–350 g; Centre d'Élevage René Janvier) were kept in thermoregulated, humidity-controlled facilities under a cycle of 12 h of light and 12 h of dark (lights on between 7:00 AM and 7:00 PM) and were allowed free access to food and water. All studies were conducted in accordance with the French legislation and European directives.

For surgery, anesthesia was induced by 5% isoflurane and maintained by 2.0%−2.5% isoflurane in 70%/30% NO$_2$/O$_2$. Half a microliter of (R,S)-α-amino-3-hydroxy-5-methyl-4-isoxazolo-propionique (AMPA) (15 mM in phosphate-buffered saline; Sigma) was stereotactically injected in the right striatum (bregma + 0.7 mm; 2.7 mm from the sagittal suture and 5.5 mm from the brain surface) using a 1-μL microsyringe and micropump (injection rate, 0.5 μL/min; UltraMicroPump II and Micro4 Controller; WPI Inc.). The animals were maintained normothermic using a heating blanket (Homeothermic Blanket Control Unit; Harvard Apparatus Limited).
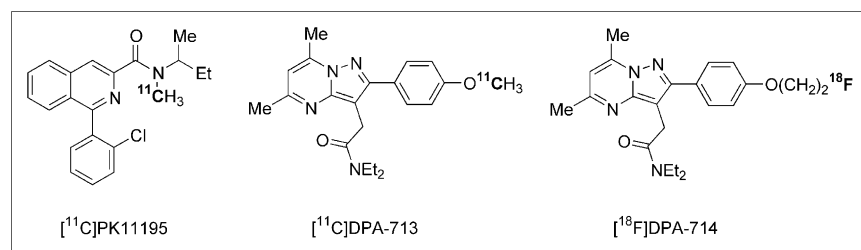
Radiosynthesis of Ligands

Racemic PK11195 and its enantiomerically pure R-isomer ((R)-PK11195, enantiomeric excess > 95%) were kindly provided by Sanofi-Aventis. DPA-713 was synthesized as previously described (13). DPA-714 was resynthesized in 2 chemical steps from DPA-713 as previously described (12) and obtained in a 32% overall yield. Nor-(R)-PK11195 ((R)-N-(1-methylpropyl)-1-(2-chlorophenyl)isoquinoline-3-carboxamide) as a precursor for the labeling of (R)-PK11195 with ^{11}C was kindly provided by Sanofi-Aventis. Nor-DPA-713 (N,N-diethyl-2-[2-(4-hydroxyphenyl)-5,7-dimethylpyrazolo[1,5-α]pyrimidin-3-yl]acetamide) as a precursor for the labeling of DPA-713 with ^{11}C was synthesized as previously described (13). N,N-diethyl-2-(2-(4-(2-toluenesulfonyloxyethoxy)-phenyl)-5,7-dimethylpyrazolo[1,5-α]pyrimidin-3-yl)acetamide, as a precursor for the labeling of DPA-714 with ^{18}F, was synthesized in 2 chemical steps from DPA-713 and obtained in a 42% yield.

(R)-PK11195 was labeled with [11]C (half-life, 20.38 min) at its amide moiety using the methylation reagent ^{11}C-methyl iodide according to slight modifications of procedures already reported (6,14). Typically, about 4.80 GBq of (R)-^{11}C-PK11195 (>98% radiochemically pure) were routinely obtained within 25 min of radiosynthesis (including high-performance liquid chromatography [HPLC] purification and formulation), with specific radioactivities ranging from 75 to 90 GBq/μmol.

DPA-713 was labeled with [11]C (half-life, 20.38 min) at its aromatic methoxy moiety from the corresponding phenolic precursor using ^{11}C-methyl triflate according to procedures already reported (15). Typically, about 7.40 GBq of ^{11}C-DPA-713 (>98% radiochemically pure) were routinely obtained within 20 min of radiosynthesis (including HPLC purification and formulation), with specific radioactivities ranging from 70 to 90 GBq/μmol.

DPA-714 was labeled with [18]F (half-life, 109.8 min) at its 2-fluoroethyl moiety using a tosyloxy-for-fluorine nucleophilic aliphatic substitution, on the basis of a previous publication (12). This simple 1-step process has been automated on our Zymate-XP (Zymark) robotic system and involves reaction of K-^{18}F-F-Kryptofix222 with the tosyloxy precursor (4.5–5.0 mg, 8.2–9.1 μmol) at 165°C for 5 min in dimethyl sulfoxide (0.6 mL), followed by C-18 PrepSep cartridge (Fisher) prepurification, and finally semipreparative HPLC purification on an X-Terra RP18 (Waters) (16). Typically, about 6.5 GBq of ^{18}F-DPA-714 (>95% radiochemically

FIGURE 1. Chemical structures of the 3 TSPO radioligands evaluated.

[11C]PK11195 [11C]DPA-713 [18F]DPA-714

pure) were routinely obtained within 90 min of radiosynthesis (including HPLC purification and formulation), with specific radioactivities ranging from 37 to 148 GBq/μmol.

Autoradiography

[11]C-DPA-713 (25.5 GBq/μmol; 29 nM) and ^{18}F-DPA-714 (136 GBq/μmol; 2 nM) autoradiographic studies were performed using 20-μm brain sections from rats sacrificed 7 d after lesioning ($n = 7$ for ^{11}C-DPA-713 and 5 for ^{18}F-DPA-714). After decapitation, the brains were quickly removed and immediately frozen in isopentane in dry ice.

Using adjacent sections, we assessed specific binding for TSPO (18 kD) with an excess of unlabeled PK11195 (20 μM), and we checked specificity for central benzodiazepine binding sites with an excess of unlabeled flumazenil (20 μM). Sections were incubated for 20 min in Tris buffer (Trizma preset crystals; Sigma [adjusted at pH 7.4 at 4°C, 50 mM, with 120 mM NaCl]) and then were rinsed 2 times for 2 min with cold buffer, followed by a quick wash in cold distilled water. Sections were then placed in direct contact with a Phosphor-Imager screen (Molecular Dynamics) and exposed overnight.

Autoradiograms were visualized and analyzed using Image-Quant software (Molecular Dynamics). A region of interest (ROI) was manually drawn on the core of the lesion, and an identical area was drawn symmetrically on the contralateral hemisphere. Binding in the ROI is expressed as the number of counts per surface unit. To compare the binding independently of the specific radioactivity of the 2 radioligands, we normalized the binding of ^{11}C-DPA-713 and ^{18}F-DPA-714 in the lesion to 100%. To that end, the contralateral binding (same brain section), as well as contra- and ipsilateral binding after displacement (adjacent brain sections), was calculated relative to the amount of tracer binding in the lesion and expressed as a percentage.

Metabolite Analysis in Rat Blood and Brain

Naive or operated adult male Wistar rats were injected in the tail vein with ^{18}F-DPA-714 (51.8–130 MBq). The animals were perfused with saline and sacrificed 20, 40, or 60 min later. A blood sample was collected, and plasma was isolated by centrifugation (5 min, 3,000 rpm). Plasma proteins were precipitated from 400 μL of serum by the addition of 400 μL of CH_3CN. After centrifugation (5 min, 3,000 rpm), the supernatant was injected onto the HPLC column. The brains were removed, and the hemispheres were separated. Homogenization by sonication was performed in 1 mL of CH_3CN per hemisphere. After rapid centrifugation, the supernatant was separated from the pellet and concentrated under reduced pressure before injection onto the HPLC column. HPLC was performed at room temperature using a 600 Controller (Waters), an 1100 Series ultraviolet detector (Hewlett Packard), a Flow One scintillation detector (Packard), and a semipreparative C18 Bondapak column (Waters) (300 × 7.8 mm; porosity, 10 μm). Solvent A was 0.1% aqueous trifluoroacetic acid, solvent B was CH_3CN, gradient elution (A/B) was 80:20 to 20:80 in 10 min, followed by 5 min at 20:80, flow rate was 4 mL/min, and absorbance detection was at a λ of 263 nm.

A similar protocol for the study of the ^{11}C-DPA-713 metabolite was previously described and involved animals sacrificed 10, 20, and 30 min after injection of ^{11}C-DPA-713 (88.0–158 MBq) (11).

PET Scans and Data Acquisition

Thirty-one rats ($n = 5$ for ^{11}C-PK11195, 12 for ^{11}C-DPA-713, and 14 for ^{18}F-DPA-714) were used for PET 7 d after AMPA injection. Anesthesia was induced by 5% isoflurane and maintained by 2.0%−2.5% isoflurane in 70%/30% NO_2/O_2. During imaging, the head of each rat was fixed in a homemade stereotactic frame compatible with PET acquisition and the rats were maintained normothermic using a heating blanket (Homeothermic Blanket Control Unit). A 24-gauge catheter in the tail vein was used for intravenous administration of all compounds.

PET was performed on a Focus 220 (Concorde), which is a dedicated small-animal scanner. Radiolabeled tracers were injected concomitantly with the start of PET acquisition, and for displacement experiments, unlabeled compounds (PK11195, DPA-713, and DPA-714, 1 mg/kg) were injected 20 min after injection of the radiotracers. PET data were acquired for 70 min after radiotracer injection. The acquisition protocol consisted of a time coincidence window set to 6 ns and energy discrimination levels set to 350 and 750 keV. The data files for the list-mode acquisition were displayed as 3D sinograms with a maximum ring difference of 47 and a span of 3. For ^{11}C-DPA-713 and ^{11}C-PK11195, the list-mode data of the emission scans were sorted into 14 or 26 frames for, respectively, control and displacement studies. Similarly, PET experiments with ^{18}F-DPA-714 were performed with 24 or 29 dynamic frames. The attenuation correction factors were measured using an external [68]Ge point source in ^{11}C-DPA-713 and ^{11}C-PK11195 experiments, and they were calculated from the emission in ^{18}F-DPA-714 experiments. Finally, the emission sinograms (i.e., each frame) were normalized, corrected for attenuation and radioactivity decay, and reconstructed using Fourier rebinning and ordered-subsets expectation maximization, 2-dimensional (16 subsets and 4 iterations).

Image Analysis

PET image analysis was performed using ASIPro VM (CTI Concorde Microsystems), a set of tools for analysis, system setup, and diagnostics. A spheric ROI of fixed size (10 mm³) was manually positioned in the center of the striatal lesion defined on a summed image of the first 25 min of each experiment (control or displacement). This ipsilateral ROI was copied and symmetrically pasted into the contralateral striatum to yield a contralateral ROI of identical volume and shape. Time–activity curves were calculated as a mean of the ROI and normalized for the percentage injected dose (%ID) per cubic centimeter.

PET Data Modeling

The simplified reference-tissue model (SRTM) (17) from the PMOD software package (version 2.5; PMOD Technologies Ltd.) was used to assess BP in the ipsilateral ROI. This model relies on a 2-tissue reversible compartment for the target region (ipsilateral ROI) and a single-tissue compartment for the reference region (contralateral ROI). Three parameters were estimated for each kinetic: R_1 (K_1/K'_1), which represents the ratio of tracer delivery; k_2, which is the clearance from the target tissue back to the vascular compartment; and BP (k_3/k_4).

Statistical Analysis

All data are expressed as mean ± SD. Comparisons were performed using ANOVA followed by a Holm–Sidak post hoc test for autoradiographic, PET and modeling data.
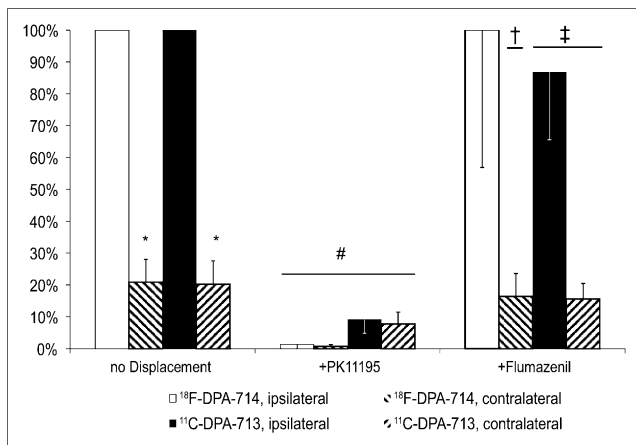
FIGURE 2. Quantification of ^{11}C-DPA-713 and ^{18}F-DPA-714 autoradiography performed on brain sections, relative to lesion binding. Error bars indicate SD. *Significantly increased binding in lesion, as compared with binding in intact tissue, $P < 0.001$. #Significant displacement by PK11195, $P < 0.01$. †Significant displacement of ^{18}F-DPA-714 in intact tissue, $P < 0.01$. ‡Significant displacement of ^{11}C-DPA-713 in intact tissue and lesion, $P < 0.01$.

RESULTS

Autoradiography

[11]C-DPA-713 and ^{18}F-DPA-714 autoradiography was performed on brain sections of rats sacrificed 1 wk after induction of neuroinflammation by intrastriatal injection of AMPA. A 10^3- to 10^4-fold excess of PK11195 (20 μM) or flumazenil (20 μM) was coincubated with, respectively, ^{11}C-DPA-713 (20 nM) and ^{18}F-DPA-714 (2 nM). Figure 2 shows the resulting quantification relative to the lesion area.

For both ^{11}C-DPA-713 and ^{18}F-DPA-714, binding was significantly higher on the ipsilateral than the contralateral side ($P < 0.001$; Fig. 2): the ratio of radiotracer in the ipsilateral versus the contralateral intact area was 5.5 ± 1.8 for ^{11}C-DPA-713 and 5.4 ± 2.0 for ^{18}F-DPA-714. For both radiotracers, the contrast between inflamed and intact areas was reduced (ipsilateral vs. contralateral areas, $P > 0.05$) by coincubation with an excess of PK11195. The reduction in binding was significant ($>90\%$, $P < 0.01$) in the ipsilateral area (Fig. 2), and a reduction was also observed in the contralateral area (a 95% decrease for ^{18}F-DPA-714 but a 60% decrease for ^{11}C-DPA-713, $P < 0.01$; Fig. 2). Flumazenil significantly ($P < 0.01$) diminished the binding of ^{11}C-DPA-713 by 10% in the ipsilateral area (Fig. 2) and up to 20% in the contralateral area, whereas the reduction of ^{18}F-DPA-714 binding by flumazenil was observed only on the contralateral side (20% decrease, $P < 0.01$; Fig. 2).

Metabolism

After intravenous injection of ^{18}F-DPA-714 in naive or operated rats, only the intact radioligand was detected in the perfused brain up to 60 min after injection (retention time, 9.7 min). One radiolabeled metabolite, more hydrophilic than ^{18}F-DPA-714, was detected in the plasma (retention time, 3.2 min) together with the parent compound. The parent compound represented 75%, 63%, and 14% of total radioactivity in the plasma after 20, 40, and 60 min, respectively. No lipophilic compounds were eluted after thorough washing of the HPLC column. As previously reported, ^{11}C-DPA-713 metabolism led to the formation of 2 hydrophilic compounds in plasma (retention times: 2.1 and 3.0 min; parent compound: 7.3 min [73% and about 60% of total radioactivity after 10 and 30 min, respectively]) which were not detected in brain tissue up to 30 min after injection of the radiotracer (11).

TABLE 1. Experimental Parameters and Results of In Vivo Imaging Studies

Radiotracer (no. of rats)	^{11}C-PK11195 (n = 5)	^{11}C-DPA-713 (n = 4)	^{11}C-DPA-713 (n = 4)	^{11}C-DPA-713 (n = 4)	^{18}F-DPA-714 (n = 5)	^{18}F-DPA-714 (n = 5)	^{18}F-DPA-714 (n = 4)
Weight (g)	275 ± 50	300 ± 10	306 ± 7	345 ± 38	344 ± 26	348 ± 32	358 ± 14
Temperature (°C)	36.6 ± 0.8	36.9 ± 0.2	36.7 ± 0.2	36.9 ± 0.2	37.0 ± 0.3	36.9 ± 0.5	36.8 ± 0.1
Injected dose (MBq)	95.3 ± 15.1 (72.2–110)	72.4 ± 7.3 (61.9–77.8)	66.5 ± 6.7 (61.1–75.9)	77.4 ± 10.1 (69.3–90.7)	69.3 ± 6.3 (61.3–75.9)	70.8 ± 9.1 (62.4–85.6)	70.2 ± 8.3 (65.1–82.5)
Specific radioactivity (MBq/nmol)	30.6 ± 24.2 (3.78–56.9)	60.9 ± 23.1 (42.2–92.4)	46.3 ± 5.2 (40.0–51.8)	55.4 ± 20.1 (38.6–81.4)	87.9 ± 64.0 (26.5–154)	37.1 ± 24.8 (8.3–67.4)	51.4 ± 31.0 (21.8–92.9)
Amount of radioligand (nmol)	8.23 ± 9.41 (1.88–23.7)	1.33 ± 0.50 (0.67–1.74)	1.41 ± 0.21 (1.25–1.71)	1.51 ± 0.47 (1.11–2.07)	1.27 ± 1.10 (0.40–2.50)	3.34 ± 2.99 (0.98–8.20)	1.75 ± 0.95 (0.89–3.00)
Mean ratio, ipsilateral/ contralateral	2.27 ± 0.08	3.31 ± 0.31	Displacement by PK11195 after 20 min: 1.2 ± 0.3 mg/kg	Displacement by DPA-713 after 20 min: 1.0 ± 0.1 mg/kg	4.30 ± 0.30	Displacement by PK11195 after 20 min: 1.4 ± 0.8 mg/kg	Displacement by DPA-714 after 20 min: 1.0 ± 0.1 mg/kg
R_1	1.10 ± 0.06	1.30 ± 0.27			1.64 ± 0.27		
k_2	0.30 ± 0.13	0.32 ± 0.20			0.46 ± 0.32		
BP	1.07 ± 0.21	2.19 ± 0.65			3.08 ± 0.67		

R_1, k_2, and BP are, respectively, ratio of tracer delivery in ipsilateral over contralateral areas, clearance, and BP. Results are expressed as mean ± SD (minimum–maximum values).

PET and Modeling

The animals were scanned 7 d after intrastriatal injection of AMPA. Experimental parameters are presented in Table 1. Both ^{11}C-DPA-713 and ^{18}F-DPA-714 showed an increased uptake of radioactivity in the ipsilateral area, as compared with the contralateral side (Figs. 3A–3C). ^{11}C-PK11195 and ^{18}F-DPA-714 uptake in the inflammatory area reached a peak within 2 min after the bolus injection and slowly decreased thereafter. In contrast, ^{11}C-DPA-713 uptake culminated at 6–10 min after injection and decreased faster afterward. In the intact brain region, all radiotracers displayed similar time–activity curves, with a peak of radioactivity followed by exponential washout.

Cerebral uptake (radioactivity values per volume) was directly compared at 6 and 62.5 min after injection, 2 time points corresponding to identical frames of PET data acquisition for all radiotracers. Uptake of ^{18}F-DPA-714 in the ipsilateral area was significantly higher than that of ^{11}C-PK11195 and ^{11}C-DPA-713 at 62.5 min ($P < 0.05$). In contrast, uptake of ^{11}C-PK11195 in the contralateral area was higher than that of ^{11}C-DPA-713 and ^{18}F-DPA-714 at

all time points, although the difference reached statistical significance at 6 min ($P < 0.05$) but not at 62.5 min. For all radiotracers, the ratio of uptake in the ipsilateral area over that in the contralateral area increased till 20 min after injection and reached a plateau thereafter (Fig. 3D); this time point was used for subsequent displacement studies. Between 20 and 70 min after injection, the uptake ratio was higher for ^{18}F-DPA-714 (4.30 ± 0.30, $P < 0.001$) than for ^{11}C-DPA-713 (3.31 ± 0.31, $P < 0.001$) or ^{11}C-PK11195 (2.27 ± 0.08, $P < 0.001$).

The time–activity curves were modeled using SRTM (17); the results are summarized in Figure 4. Calculation of the ratio of transport rate from blood to brain tissue, R_1 (K1/K′1) and of BP using SRTM was reliable, with a coefficient of variation generally below 10% for each R_1 and BP value. R_1 values were close to unity for ^{11}C-PK11195 ($R_1 = 1.10 \pm 0.06$) and ^{11}C-DPA-713 (1.30 ± 0.27, $P = 0.2$), whereas they were significantly higher for ^{18}F-DPA-714 ($R_1 = 1.64 \pm 0.27$, $P < 0.001$). The BP of ^{18}F-DPA-714 (3.08 ± 0.67) was significantly higher than that of ^{11}C-DPA-713 (2.19 ± 0.65, $P < 0.05$), itself greater
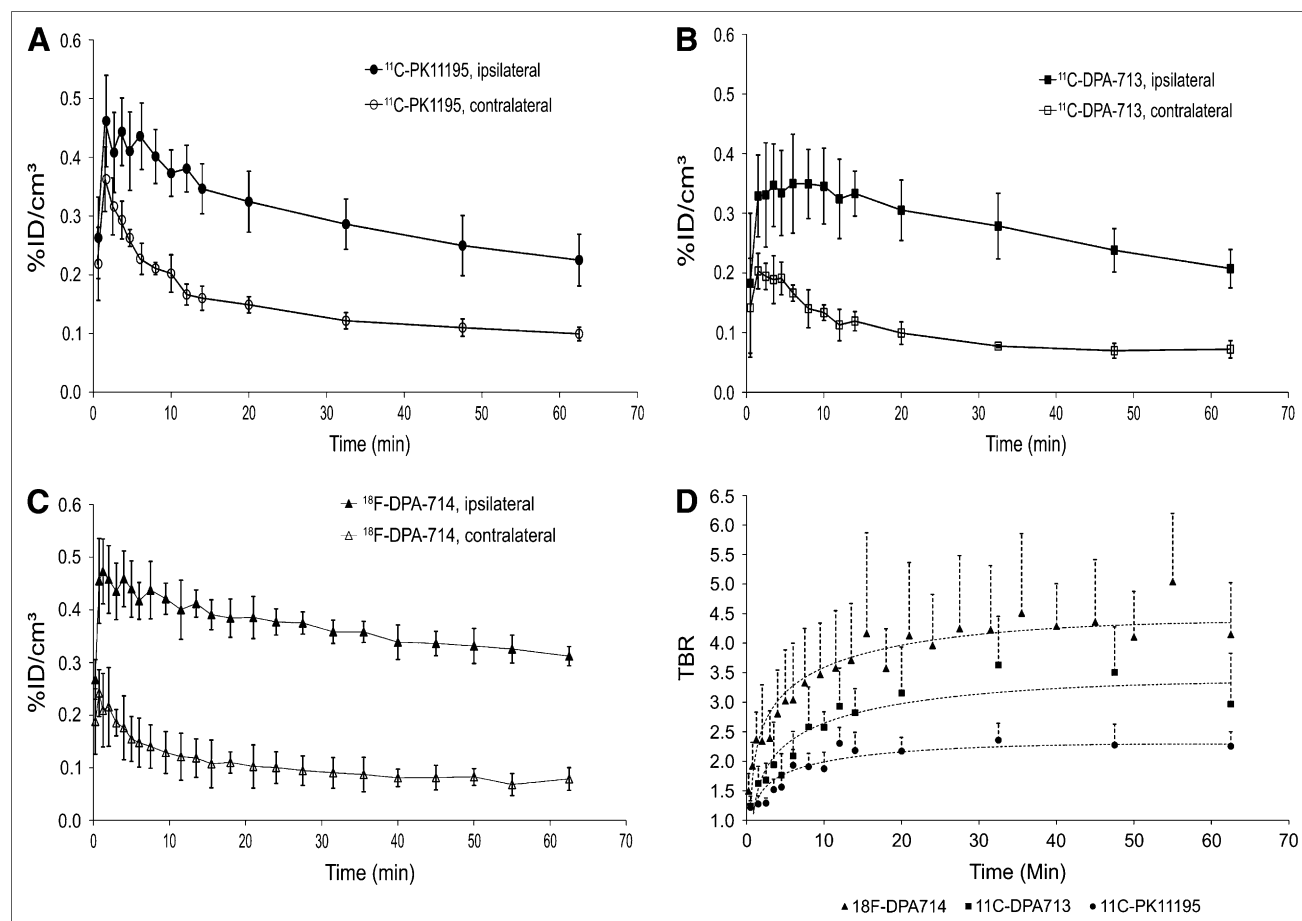
FIGURE 3. (A–C) Time–activity curves of ROI placed on lesion or on contralateral control hemisphere in rats bearing striatal lesion and injected with ^{11}C-PK11195 (A), ^{11}C-DPA-713 (B), or ^{18}F-DPA-714 (C). (D) Corresponding ratio of target (lesion) to background (control) for the 3 tracers, and exponential fit of points.
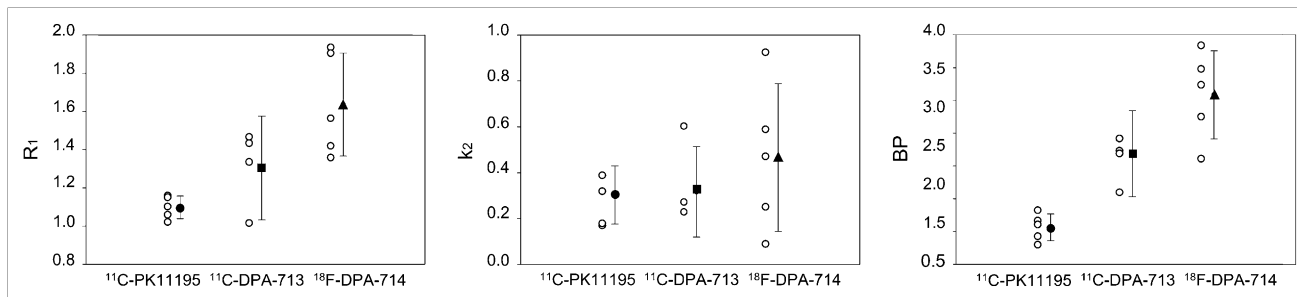
FIGURE 4. R_1, k_2, and BP obtained from ^{11}C-PK11195, ^{11}C-DPA-713, and ^{18}F-DPA-714 PET data, using SRTM. Open circles = individual values; solid symbols and error bars = mean ± SD.

than the BP of ^{11}C-PK11195 (1.07 ± 0.21, $P < 0.01$). Clearance (k_2) determination exhibited a higher uncertainty (coefficient of variation between 10% and 20%) with this model, but no differences were found between the radiotracers.

Because ^{11}C-DPA-713 and ^{18}F-DPA-714 had tracer delivery ratio values (R_1) higher than 1, we wanted to examine the influence of an increased R_1 on the corresponding BP. This was done by simulating the modeling with a hypothetical R1 in the range of 0.9–1.1. For both radioligands, the hypothetical BP values showed no significant difference from the former ones (^{11}C-DPA-713: 2.08 ± 0.53 vs. 2.19 ± 0.65, $P < 0.05$; ^{18}F-DPA-714: 2.91 ± 0.71 vs. 3.08 ± 0.67, $P < 0.05$) but remained significantly greater than the BP of ^{11}C-PK11195 ($P < 0.01$).

Displacement studies were performed by injection of an excess (1 mg/kg) of either PK11195 or the nonradiolabeled reference compound, exactly 20 min after tracer injection. This induced a fast decline of both ^{11}C-DPA-713 and ^{18}F-DPA-714 concentrations in the lesion. Five to 10 min after displacement, time–activity curves in the ipsilateral and contralateral areas were superimposed (Fig. 5), and the images showed a loss of contrast in the rat brain (Fig. 6).

DISCUSSION

The large number (more than 40) of candidate TSPO radiotracers radiolabeled over the past few years (9) highlights the strong interest in quantitative imaging of the inflammatory reaction in the brain and calls for an efficient and rigorous evaluation of these molecules in animal models for clinical applications in neurologic disorders such as stroke and neurodegenerative diseases. Direct in vivo comparison between a candidate TSPO radiotracer and the reference radiotracer ^{11}C-PK11195 in similar neuroinflammatory conditions has been published for ^{11}C-CLINME (18) but was not completed for ^{11}C-DAA1106, for which in vivo imaging of rats with striatal lesion was not quantified (19). Other radioligands such as ^{11}C-VC195 (20) or ^{18}F-PK14105 (21) were found to perform as well as ^{11}C-PK11195 in similar rat models, as examined ex vivo by microdissection of the brain. Alternatively, brain imaging in

primates and in humans has been reported for several promising peripheral benzodiazepine receptor radiotracers (e.g., ^{18}F-FEDAA1106, ^{11}C-peripheral benzodiazepine receptor 28, and ^{11}C-vinpocetine (9)), but biodistribution in healthy animals provides limited information on capacity to detect microglial activation.

^{18}F-DPA-714 is a TSPO radioligand labeled with [18]F (109.8 min), a preferred PET isotope for radiopharmaceutical chemistry. In the present study, we investigated ^{18}F-DPA-714 in an acute rat model of neuroinflammation and compared its PET imaging profile with that of ^{11}C-DPA-713 and ^{11}C-PK11195 in the same model. Until now, this radioligand has been evaluated only ex vivo on rat brain sections with a unilateral striatal lesion and in vivo in the healthy baboon (12).

As previously described (11,18), injection of 7.5 nmol of AMPA in the right striatum causes neuronal loss, strong astroglial activation, and macrophage recruitment. This robust neuroinflammatory reaction has been extensively characterized by immunohistochemistry at 7 d after lesioning, the time at which PET was performed, showing a dense cluster of CD11b-reactive cells (activated microglia and infiltrated monocytes/macrophages) surrounded by a clear astrocytic (glial fibrillary acidic protein–reactive) scar isolating the lesion from the surrounding healthy tissue (11,18). However on the contralateral intact side, neither microglial nor astrocytic activation was detectable by immunohistochemistry. This neuroinflammation model is considered an efficient screening tool for the evaluation of new TSPO radioligands (9).

In vitro autoradiography confirmed that the AMPA lesion gave rise to a well-defined TSPO-rich lesion that could be easily and similarly visualized using either ^{11}C-DPA-713 or ^{18}F-DPA-714 and enhanced radiotracer binding by more than 5-fold in the ipsilateral area as compared to the contralateral tissue. The contrast between ipsilateral and contralateral areas disappeared in the presence of an excess of PK11195, demonstrating the specificity of the binding toward TSPO. PK11195 also reduced the binding of ^{11}C-DPA-713 and ^{18}F-DPA-714 on the contralateral side, with a respective decrease of 60% and more than 95% of the
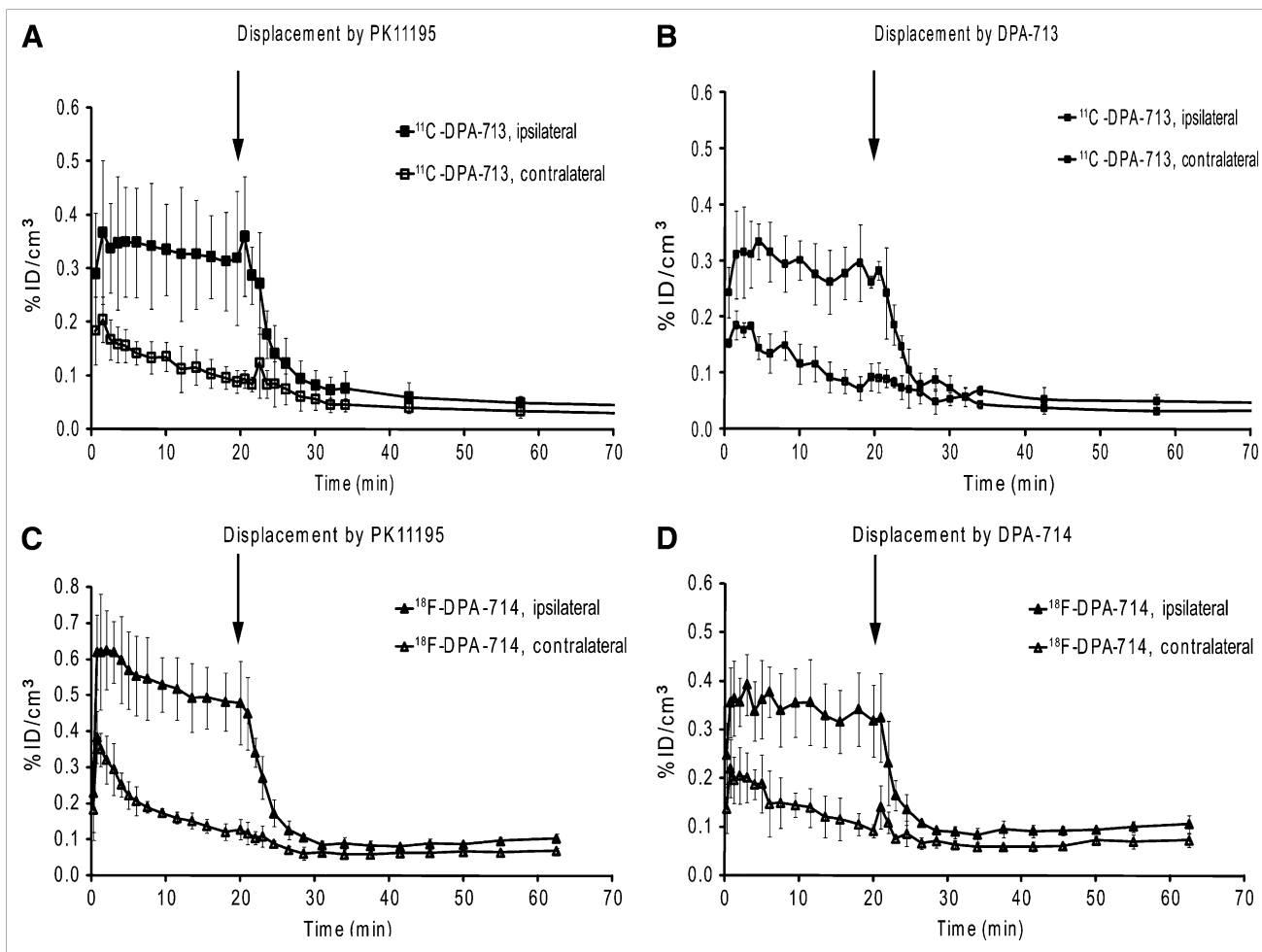
FIGURE 5. Displacement experiments: ^{11}C-DPA-713 injection followed by PK11195 (A) or DPA-713 (B), and ^{18}F-DPA-714 injection followed by PK11195 (C) or DPA-714 (D). Arrows indicate time of displacement, 20 min after radiotracer injection.

initial values, highlighting detectable TSPO-specific binding in the noninflammatory areas of the brain. This decrease was significantly larger for ^{18}F-DPA-714 than for ^{11}C-DPA-713, possibly because of different levels of nonspecific binding or different experimental conditions, such as the specific radioactivity. Indeed, the concentration ratio of PK11195 coincubated with ^{18}F-DPA-714 was 10 times higher than that for coincubation with ^{11}C-DPA-713 (a 10,000-fold excess, compared with a 1,000-fold excess).

An excess of flumazenil, a ligand specific for central benzodiazepine receptors (CBRs), did not prevent visualization of the inflamed area, although the binding of ^{11}C-DPA-713 was significantly affected in both the ipsilateral and the contralateral areas. This result suggests a significant in vivo affinity of ^{11}C-DPA-713 for CBR, although the inhibition constant values of DPA-713 toward ^{3}H-flumazenil as measured in vitro in rat cerebral cortex membranes or rat kidney mitochondrial membranes showed a negligible affinity (>10,000 nM) for CBR (*12,22*). Alternatively, flumazenil could share nonspecific (non-TSPO and non-CBR)

binding sites with ^{11}C-DPA-713. With ^{18}F-DPA-714, displacement by flumazenil was observed only in the contralateral area, also indicative of in vivo affinity toward CBR, though again inhibition constant values obtained in vitro showed negligible affinity for the central receptor (*12,22*).

Overall, autoradiography with ^{11}C-DPA-713 and ^{18}F-DPA-714 confirmed TSPO specificity in the inflammatory region and suggests that basal uptake in intact brain tissue is only partly TSPO-specific.

To quantify radiotracer uptake on PET images, we designed a spheric ROI of a constant volume in the core of the inflammatory zone. Because this method takes into account the interindividual variability of lesion size and avoids overestimation of the damaged area by partial-volume effects, we preferred this method to delineation of the entire lesion as it appears on PET images. After the injection and distribution of ^{11}C-PK11195, ^{11}C-DPA-713, and ^{18}F-DPA-714, uptake was significantly higher in the ipsilateral area than in the contralateral area, allowing clear visualization of the lesion site on the PET images. Inter-
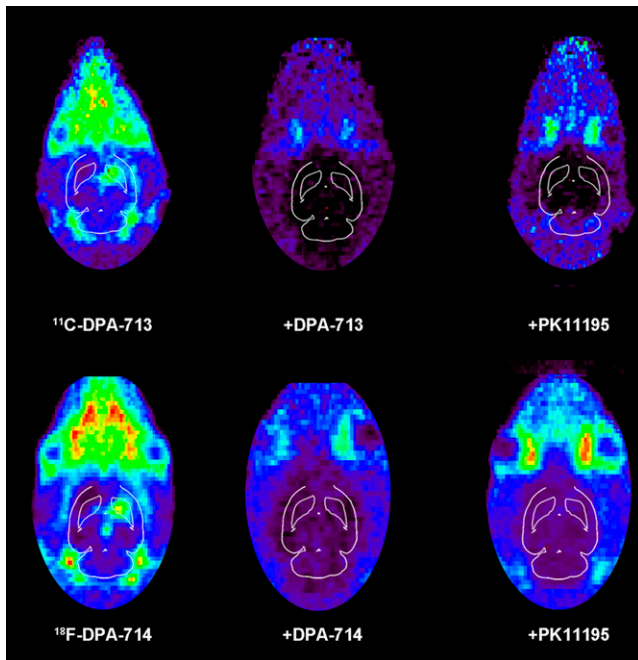
FIGURE 6. Normalized PET images (%ID/cm³, horizontal plane) at level of striatal lesion. Top row from left to right: summed images of ¹¹C-DPA-713 in control study (0–70 min) and after displacement by DPA-713 or PK11195 (30–70 min); bottom row from left to right: summed images of ¹⁸F-DPA-714 in control study (0–70 min) and after displacement by DPA-714 or PK11195 (30–70 min).

estingly, ¹⁸F-DPA-714 achieved a higher uptake than did ¹¹C-PK11195 and ¹¹C-DPA-713, suggesting a higher bioavailability in cerebral tissue. Both ¹¹C-DPA-713 and ¹⁸F-DPA-714 showed a lower uptake than did ¹¹C-PK11195 in the contralateral area. Because intact brain tissue expresses minimal amounts of TSPO, this result suggests that DPA ligands display a lower nonspecific binding than does ¹¹C-PK11195 in vivo, a characteristic that could be related to their lower lipophilicity than that of PK11195. Overall, ¹⁸F-DPA-714 demonstrated the best performance as shown by the highest ratio of ipsilateral uptake to contralateral uptake and the highest BP after modeling of time–activity curves using SRTM. ¹¹C-DPA-713, although not performing at the level of ¹⁸F-DPA-714, also performed better than ¹¹C-PK11195, and differences between the 3 radiotracers were significant using both types of analyses (ratio and BP).

Both ¹⁸F-DPA-714 and ¹¹C-DPA-713 were rapidly and completely displaced from the ipsilateral area by an excess of the corresponding unlabeled compound or PK11195, reaching within minutes the level of uptake in the contralateral intact area. This result demonstrates the specificity of the contrast obtained in vivo with PET.

Modeling with SRTM highlighted that ¹⁸F-DPA-714 and ¹¹C-DPA-713 had higher BP and tracer delivery ratio (R_1) values than did ¹¹C-PK11195. Values of R_1 ($K_1 > K_1'$) higher than 1 indicate a facilitated entry of the radiotracer in the target area (ipsilateral area) with respect to the reference area (contralateral area) and bring into question the state of the blood–brain barrier and its influence on the final uptake of radiotracers in the lesion. Despite the absence of any Evans blue permeation at the time of the PET scan in this model (*11,18*), the blood–brain barrier may nevertheless be modified such that entry of more polar ligands (compared with ¹¹C-PK11195) into the lesion would be favored over entry into healthy tissue. To cope with this potential bias, we simulated each individual ¹⁸F-DPA-714 and ¹¹C-DPA-713 PET examination using the SRTM, imposing a hypothetical value of tracer delivery ratio R_1 that was constrained between 0.9 and 1.1. Hypothetical BP values for ¹⁸F-DPA-714 and ¹¹C-DPA-713 were not significantly different from real BP values, showing that differences in R_1 that affect mainly the distribution phase have a limited influence on the BP achieved by a particular radioligand. Alternatively, an increased blood flow in the lesion could be responsible for these variations in radioligand transport rate.

Validation of SRTM, however, requires comparison with plasma input models, which remain technically difficult in rodents. Overall, STRM appears reasonable for this animal model, as the method gives rise to focal enhancement of a receptor negligibly expressed in normal brain tissue.

The absence of detectable brain metabolism of the molecules ensures that the quantification of PET images adequately reflects the potential of these radiotracers to serve as biomarkers for neuroinflammation imaging. Because ¹¹C-DPA-713 and ¹⁸F-DPA-714 were shown to be equally potent in detecting activated microglial cells on brain slices (in vitro autoradiography), the higher in vivo contrast of ¹⁸F-DPA-714 than of ¹¹C-DPA-713 may be attributed to a more favorable biodistribution.

Excitotoxic models create a robust neuroinflammatory reaction that facilitates preliminary examination of new radioligands, but the results may not be extrapolated to milder neuroinflammatory conditions, such as those generally encountered in neuropathologic diseases. This limitation of the current study calls for further investigations of ¹¹C-DPA-713 and ¹⁸F-DPA-714 in other animal models of stroke or neurodegenerative diseases.

CONCLUSION

Although not representative of a clinical situation, the intracerebral AMPA lesion in rats is a robust model for preclinical screening of different TSPO candidate radiotracers and allowed us to demonstrate that ¹⁸F-DPA-714 performed better overall than ¹¹C-DPA-713 or ¹¹C-PK11195. This finding, together with the ease of labeling with ¹⁸F, suggests that ¹⁸F-DPA-714 is a promising TSPO radiotracer for PET. Further work with ¹⁸F-DPA-714 should include longitudinal evaluation of other neuroinflammatory conditions to test whether the higher BP values reported here translate into a higher sensitivity for the detection of microglial activation.

REFERENCES

1. Nguyen MD, Julien JP, Rivest S. Innate immunity: the missing link in neuroprotection and neurodegeneration? *Nat Rev Neurosci.* 2002;3:216–227.
2. Benavides J, Capdeville C, Dauphin F, et al. The quantification of brain lesions with an omega 3 site ligand: a critical analysis of animal models of cerebral ischaemia and neurodegeneration. *Brain Res.* 1990;522:275–289.
3. Chen MK, Guilarte TR. Translocator protein 18 kDa (TSPO): Molecular sensor of brain injury and repair. *Pharmacol Ther.* 2008;118:1–17.
4. Banati RB. Visualising microglial activation in vivo. *Glia.* 2002;40:206–217.
5. Cagnin A, Kassiou M, Meikle SR, Banati RB. Positron emission tomography imaging of neuroinflammation. *Neurotherapeutics.* 2007;4:443–452.
6. Camsonne R, Crouzel C, Comar D, et al. Synthesis of N-(C-11) methyl, N-(methyl-1 propyl), (chloro-2 phenyl)-1 isoquinoline carboxamide-3 (PK11195): a new ligand for peripheral benzodiazepine receptors. *J Labelled Comp Radiopharm.* 1984;21:985–991.
7. Venneti S, Lopresti BJ, Wiley CA. The peripheral benzodiazepine receptor (translocator protein 18kDa) in microglia: from pathology to imaging. *Prog Neurobiol.* 2006;80:308–322.
8. James ML, Selleri S, Kassiou M. Development of ligands for the peripheral benzodiazepine receptor. *Curr Med Chem.* 2006;13:1991–2001.
9. Chauveau F, Boutin H, Van Camp N, Dollé F, Tavitian B. Nuclear imaging of neuroinflammation: a comprehensive review of [^{11}C]PK11195 challengers. *Eur J Nucl Med Mol Imaging.* 2008;35:2304–2319.
10. Benavides J, Quarteronet D, Imbault F, et al. Labelling of "peripheral-type" benzodiazepine binding sites in the rat brain by using [^{3}H]PK 11195, an isoquinoline carboxamide derivative: kinetic studies and autoradiographic localization. *J Neurochem.* 1983;41:1744–1750.
11. Boutin H, Chauveau F, Thominiaux C, et al. ^{11}C-DPA-713: a novel peripheral benzodiazepine receptor PET ligand for in vivo imaging of neuroinflammation. *J Nucl Med.* 2007;48:573–581.
12. James ML, Fulton RR, Vercoullie J, et al. DPA-714, a new translocator protein-specific ligand: synthesis, radiofluorination, and pharmacologic characterization. *J Nucl Med.* 2008;49:814–822.
13. James ML, Fulton RR, Henderson DJ, et al. Synthesis and in vivo evaluation of a novel peripheral benzodiazepine receptor PET radioligand. *Bioorg Med Chem.* 2005;13:6188–6194.
14. Cremer JE, Hume SP, Cullen BM, et al. The distribution of radioactivity in brains of rats given [N-methyl-^{11}C]PK 11195 in vivo after induction of a cortical ischaemic lesion. *Int J Rad Appl Instrum B.* 1992;19:159–166.
15. Thominiaux C, Dolle F, James ML, et al. Improved synthesis of the peripheral benzodiazepine receptor ligand [^{11}C]DPA-713 using [^{11}C]methyl triflate. *Appl Radiat Isot.* 2006;64:570–573.
16. Damont A, Hinnen F, Kuhnast B, et al. Radiosynthesis of [^{18}F]DPA-714, a selective radioligand for imaging the translocator protein (18 kDa) with PET. *J Labelled Comp Radiopharm.* 2008;51:286–292.
17. Lammertsma AA, Hume SP. Simplified reference tissue model for PET receptor studies. *Neuroimage.* 1996;4:153–158.
18. Boutin H, Chauveau F, Thominiaux C, et al. In vivo imaging of brain lesions with [^{11}C]CLINME, a new PET radioligand of peripheral benzodiazepine receptors. *Glia.* 2007;55:1459–1468.
19. Venneti S, Lopresti BJ, Wang G, et al. A comparison of the high-affinity peripheral benzodiazepine receptor ligands DAA1106 and (R)-PK11195 in rat models of neuroinflammation: implications for PET imaging of microglial activation. *J Neurochem.* 2007;102:2118–2131.
20. Belloli S, Moresco RM, Matarrese M, et al. Evaluation of three quinoline-carboxamide derivatives as potential radioligands for the in vivo pet imaging of neurodegeneration. *Neurochem Int.* 2004;44:433–440.
21. Price GW, Ahier RG, Hume SP, et al. In vivo binding to peripheral benzodiazepine binding sites in lesioned rat brain: comparison between [^{3}H]PK11195 and [^{18}F]PK14105 as markers for neuronal damage. *J Neurochem.* 1990;55:175–185.
22. Selleri S, Bruni F, Costagli C, et al. 2-arylpyrazolo[1,5-a]pyrimidin-3-yl acet-amides: new potent and selective peripheral benzodiazepine receptor ligands. *Bioorg Med Chem.* 2001;9:2661–2671.